Structure-Dependent Photoluminescence in Low-Dimensional Ethyl-, Propyl-, and Butylammonium Lead Iodide Perovskites

*Chang-Wei Lin,[1] Fangzhou Liu,[2] Ting-Yang Chen,[1] Kuan-Hua Lee,[1] Chung-Kai Chang,[3] Yanling He,[2,4] Tik Lun Leung,[4] Alan Man Ching Ng,[4] Chia-Hung Hsu,[1,3] Jasminka Popović,[5] Aleksandra Djurišić, [*2] and Hyeyoung Ahn[*1]*

[1]Department of Photonics, College of Electrical and Computer Engineering, National Chiao Tung University, Hsinchu 30010, Taiwan.

[2]Department of Physics, University of Hong Kong, Pokfulam Road, Hong Kong.

[3]National Synchrotron Radiation Research Center, Hsinchu 300, Taiwan.

[4]Department of Physics, Southern University of Science and Technology, No. 1088, Xueyuan Road, Shenzhen, Guangdong, China.

[5]Center of Excellence for Advanced Materials and Sensing Devices, Division for Materials Physics, Laboratory for Synthesis and Crystallography of Functional Materials, Ruđer Bošković Institute, Bijenička 54, Zagreb, Croatia.

KEYWORDS. Two-Dimensional Materials, Hybrid Lead Halide Perovskites, Alkylammonium. Excitonic Emission, Broadband Emission

ABSTRACT. Hybrid organic-inorganic perovskites have attracted great attention as the next generation material for photovoltaic and light emitting devices. However, their environment instability issue remains as the largest challenge for practical applications. Recently emerging two-dimensional (2D) perovskites with Ruddlesden–Popper (R-P) structures are found to greatly improve the stability and aging problems. Furthermore, strong confinement of excitons in these natural quantum-well structures results in the distinct and narrow light emission in the visible spectral range, enabling the development of spectrally tunable light sources. Besides the strong quasi-monochromatic emission, some 2D perovskites comprised of the specific organic cations and inorganic layer structures emit a pronounced broadband emission. Herein we report the light emitting properties and the degradation of low-dimensional perovskites consisting of the three shortest alkylammonium spacers, mono-ethylammonium (EA), *n*-propylammonium (PA), and *n*-butylammonium (BA). While $(BA)_2PbI_4$ is known to form well-oriented 2D thin films consisting of layers of corner-sharing PbI_6 octahedra separated by a bilayer of BA cations, EA with shorter alkyl chains tends to form other type of lower dimensional structure. Nevertheless, optical absorption edges of as-prepared fresh $EAPbI_3$, $(PA)_2PbI_4$, and $(BA)_2PbI_4$ are obviously blue-shifted to 2.4–2.5 eV compared to their 3D counterpart, methylammonium lead iodide ($MAPbI_3$) perovskite, and they all emit narrow excitonic photoluminescence. Furthermore, by carefully optimizing deposition conditions, we have achieved predominantly 2D structure for $(PA)_2PbI_4$. However, unlike $(BA)_2PbI_4$, upon exposure to ambient environment $(PA)_2PbI_4$ readily transforms to a different crystal structure, exhibiting a prominently broadband light from *ca*. 500 nm to 800 nm and a gradual increase in intensity as structural transformation proceeds.

INTRODUCTION

Organic-inorganic halide perovskites are a revolutionary class of semiconductors with broad solar absorption and the recent advances of perovskite-based solar cells increased the power conversion efficiency (PCE) to over 25 %.[1] However, despite excellent performance in terms of efficiency, conventional 3D halide perovskites typically exhibit inferior ambient stability. Consequently, there has been a great deal of interest in exploration of other types of halide perovskites, including various lower dimensional (2D, 1D, or 0D) perovskites. Recently, Ruddlesden–Popper (R-P) two-dimensional (2D) structures of halide perovskites have been realized by introducing organic barrier layers between inorganic main layers.[2,3] While conventional small volume methylammonium cations (CH_3NH_3, MA) in $MAPbI_3$ are enclosed in the octahedral inorganic cages, the insertion of the long-chain alkylammonium organic cations, such as butylammonium (BA), can separate octahedral layers. In the R-P 2D structures, corner-sharing PbI_6 octahedron layers separated by organic cations form an alternate inorganic–organic ⟨100⟩ -oriented 2D sheet structures. Furthermore, since the alkylammonium cations are typically hydrophobic, they improve the stability of 2D layered perovskites in ambient atmosphere.[4] Meanwhile, a new series of multi-dimensional perovskites are realized when certain intermediate size spacing cations, such as phenylalkylammonium, are incorporated in hybrid metal halide perovskites.[5-9] Among them, low-dimensional step-like structures can be formed from polymorphs of PbI_6 octahedra connected through face-sharing as well as corner-sharing methods.

Here we report the relationship between structure and optical properties of alkylammonium lead-iodide perovskites consisting of alkylammonium cations (RNH_3^+, $R=C_nH_{2n+1}$, $n \geq 2$) with different alkyl chain length; ethylammonium (EA), propylammonium (PA), and butylammonium (BA). They are three shortest alkylammonium spacing cations with only two-, three-, and four-carbon chain length. The optical absorption edges of all three perovskites are blue-shifted to

around 2.5 eV compared to a 3D $MAPbI_3$ at ~1.6 eV. The binding energies of excitons in 2D $(PA)_2PbI_4$ and $(BA)_2PbI_4$ are as high as 600–650 meV due to the exciton states in the well separated 2D layer structures, whereas the exciton binding energy of $EAPbI_3$ with face-sharing chained PbI_6 octahedra is similar to that of $MAPbI_3$. Meanwhile, different from $(BA)_2PbI_4$, $(PA)_2PbI_4$ exhibits dramatic changes in terms of crystal structure, absorption, and photoluminescence (PL) upon exposure to ambient environment. The optical absorption edge of the unencapsulated-$(PA)_2PbI_4$ (U-$(PA)_2PbI_4$) is largely blue-shifted from 2.5 eV to 2.8 eV. In addition, instead of narrow free-exciton emission, U-$(PA)_2PbI_4$ emits a broadband PL which covers nearly full visible spectrum. Such broadband emissions are typically associated with lattice deformation-induced self-trapped exciton states and have been observed only for another subset of 2D perovskites with more complex spacer cations.[10-15] Despite many recent works on alkylammonium-based low-dimensional perovskites, the broadband emission without free-exciton emission and its relation with aging-induced structural deformation have been rarely investigated from the perovskites containing only alkylammonium cations.[16-18] In our work, the enhancement of broadband emission is also observed with greater degree of structural transformation of PA-based perovskite upon exposure to ambient and it indicates that the changes in the crystal structure of U-$(PA)_2PbI_4$ favors exciton self-trapping and is advantageous in the realization of broadband optical devices.

RESULTS AND DISCUSSION

Figure 1a illustrates the top view scanning electron micrograph (SEM) of $EAPbI_3$, $(PA)_2PbI_4$ and $(BA)_2PbI_4$ films encapsulated by a thin quartz plate. Self-assembled $EAPbI_3$ film shows a granular morphology with an average grain size of ≤500 nm whereas the images of $(PA)_2PbI_4$ and $(BA)_2PbI_4$ show more uniform films with high coverage and a fine texture. The sheet-like morphologies in $(PA)_2PbI_4$ and $(BA)_2PbI_4$ characterize the growth of two-dimensional layered

films. Small grain and less interconnected crystallites in $EAPbI_3$ is similar to that of $MAPbI_3$ in the inset. Figure 1b shows the room-temperature absorption spectra of three alkylammonium perovskites and $MAPbI_3$ for comparison purposes. The absorption edges of alkylammonium perovskites are largely blue-shifted with respect to that of $MAPbI_3$, which reflects the increase of cation-halogen interaction due to the transition to lower-dimensional perovskites.[19] There are narrow excitonic absorption peaks below the band edge, which are more apparent for $(PA)_2PbI_4$ and $(BA)_2PbI_4$. The second-derivatives of absorption (d^2A) in the lower panel of Figure 1b show the resonance absorption at ~2.5 eV for three alkylammonium perovskites.

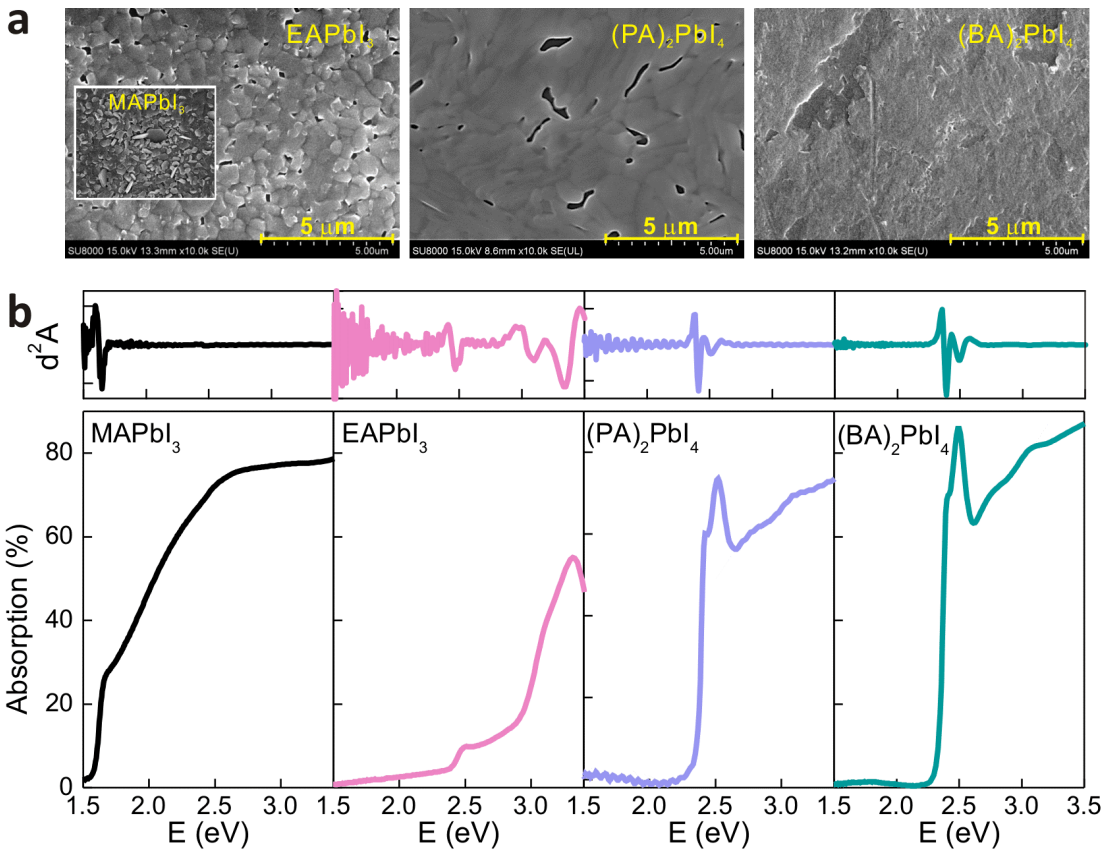

Figure 1. a. Top view SEM of the sample morphology of encapsulated $EAPbI_3$, $(PA)_2PbI_4$, and $(BA)_2PbI_4$. Inset shows the SEM image of $MAPbI_3$ for comparison purposes. **b.** The optical

absorption (lower panel) and its second-derivative (upper panel) spectra of $MAPbI_3$, $EAPbI_3$, $(PA)_2PbI_4$, and $(BA)_2PbI_4$ at room temperature, respectively.

Before investigating the optical properties, in order to understand the relation between the crystal structure and the optical properties, we first measured the Raman spectra and X-ray diffraction (XRD) of unencapsulated alkylammonium perovskites as well as $MAPbI_3$. In Figure S1, two characteristic Raman peaks are observed at 97 and 111 cm^{-1} for $MAPbI_3$. The former corresponds to Pb-I-Pb bending vibration and the latter to the Pb-I stretching.[20,21] Meanwhile, after ambient exposure within 1 week, the vibrational mode at 99 cm^{-1} of U-$(PA)_2PbI_4$ is slightly softened. The perovskite layer distortion between adjacent octahedra is determined from the Pb-I-Pb bending angles, and the increase of the angular distortion of octahedral cage in low-dimensional perovskites is known to be responsible for the weakening of the peak at 99 cm^{-1}.[14,20] Therefore, the softening of the peak at 99 cm^{-1} for aged $(PA)_2PbI_4$ manifests a higher degree of lattice deformation under the excitation of pump light.

To further investigate the crystal structure of the samples, XRD measurements were performed and the obtained results are shown in Figure 2. Le-Bail fitting was used for indexing and determination of the lattice parameters. Insets show the schematic views of crystal structure used for fitting. As expected, in Figure 2a, the utilization of MA cation results in the formation of 3D perovskite structure that crystallizes in tetragonal space group *I*4/*mcm* with refined unit-cell parameters a = 8.873(1) Å and c = 12.6948(5) Å, in good agreement with literature.[22] Meanwhile, as shown from the crystal structure in the inset of Figure 2b, the use of EA leads to the formation of structure that does not contain corner-shared PbI_6 octahedra, yet instead the one-dimensional (1D) face-shared chains running along the *b*-axis of the unit cell are formed. All reflections in Figure 2b are indexed by an orthorhombic unit cell with a = 8.611(2) Å, b = 8.026(2) Å, and c =

30.116(1) Å, similar to those reported by Park *et al.*[6] Introduction of much longer chain ligand, BA cation, produces a sharp, well-defined XRD peaks in Figure 2c, indicating the formation of a typical 2D R-P structure for $(BA)_2PbI_4$, similar to that reported by Dou *et al.*[23] By assuming an orthorhombic space group for $(BA)_2PbI_4$, the refined lattice parameters of unit-cell are determined to be $a = 8.131(4)$ Å, $b = 27.627(1)$ Å and $c = 8.272(1)$ Å. Peaks marked with "*" in Figure 2a and b correspond to ITO/glass substrates.

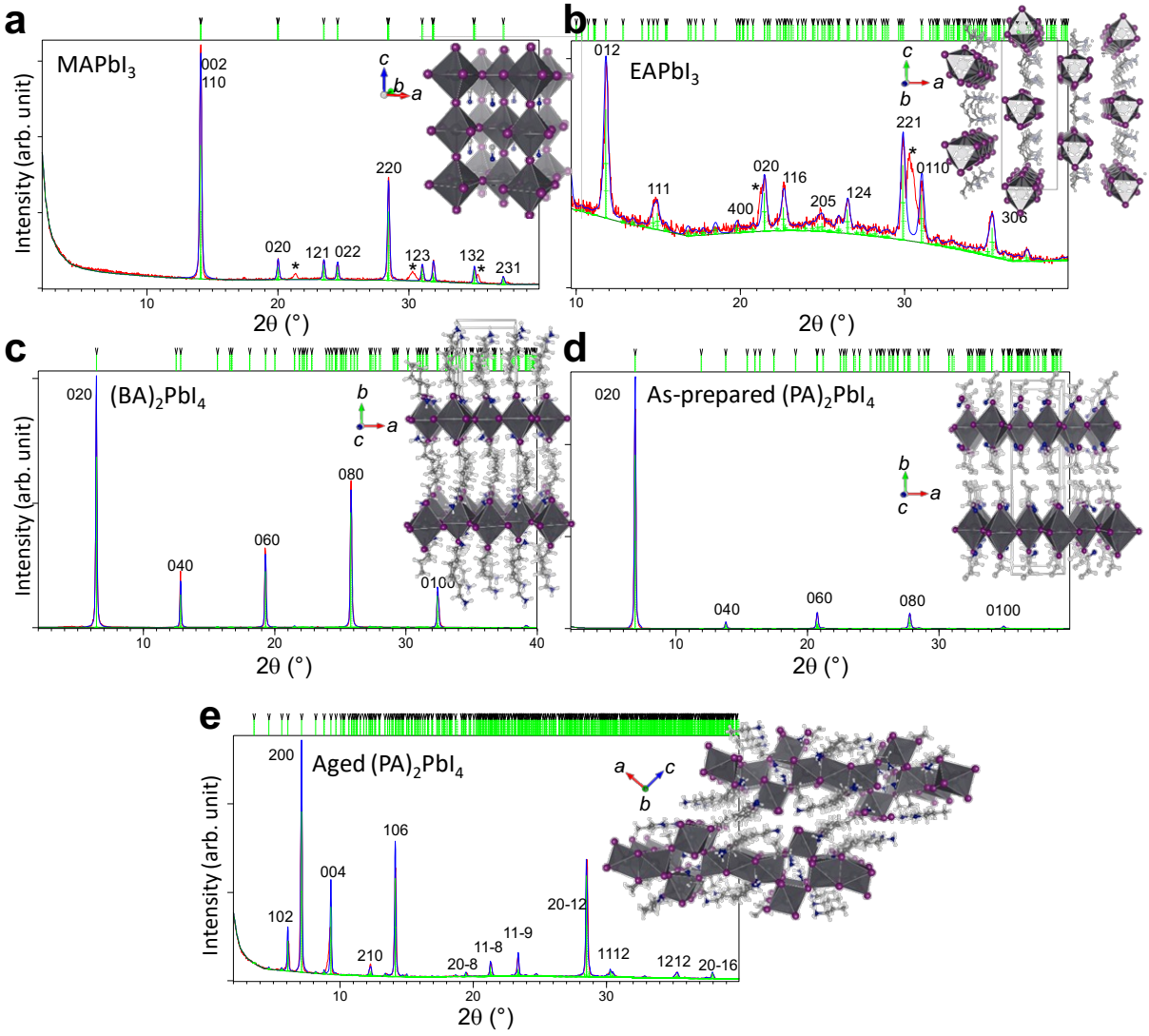

Figure 2. Le-Bail fitting on XRD data collected for **a.** $MAPbI_3$, **b.** $EAPbI_3$, **c.** $(BA)_2PbI_4$, **d.** $(PA)_2PbI_4$, and **e.** aged $(PA)_2Pb_{1.25}I_{4.5}$ in ambient environment. Inset in each figure shows the schematic view of crystal structure. Symbols in it represent Pb and its polyhedra in grey, iodide in deep purple, and nitrogen in deep blue. "*" in Figure 2a and b corresponds to peaks of ITO/glass substrate.

When PA cation with an intermediate CH_2 chain length between EA and BA is used, the 2D layered perovskite structure, similar as in the case of $(BA)_2PbI_4$, is observed in the as-prepared sample, as shown in Figure 2d. As-prepared $(PA)_2PbI_4$ crystallizes in P*nma* space group with the refined lattice parameters a = 7.919(1) Å, b = 25.670(2) Å and c = 7.878(3) Å, similar to the structure of $(PA)_2PbCl_4$ reported by Meresse and Daoud.[24] Meanwhile, Figures 2d and 2e show that the XRD patterns of as-prepared and aged PA-based samples differ significantly. Upon an ambient exposure, the as-prepared PA structure swiftly changes from the perovskite motive containing corner-shared lead iodide octahedra (Figure 2d, inset) to the complex structure containing inorganic sheets of both corner- and face-sharing $[PbI_6]^{4-}$ octahedra (Figure 2e, inset). The structure determined by Billing and Lemmerer[25] has been used as a starting structural model for the Le-Bail refinement of aged sample in Figure 2d. Lattice refinement shows that aged structure has a monoclinic space group with unit cell parameters a = 24.884(3) Å, b = 8.793(1) Å, c = 38.073(1) Å, and β = 94.57(5)°. Chemical composition derived from structural refinement points out that aged structure, in fact, does not correspond exactly to PA:Pb:I=2:1:4 as in the case of as-prepared sample, instead, the composition amounts to PA:Pb:I=2:1.25:4.5 due to presence of different connectivity modes of PbI_6 octahedra. Similar structures with face- and corner-sharing of octahedra were reported for $(PA)_7Pb_5I_{18}$ and phenylalkylammonium lead halide perovskites.[7,8] Detailed representation of specific structural features within the inorganic layer in the aged PA-

based sample are shown in Figure S2. It should be noted that with further atmosphere exposure the structural transformation and degradation of PA-based perovskite are increased, as shown in Figure S1b–S1d where many new diffraction peaks appear and become dominant as aging proceeds.

In order to understand the radiation behavior of these materials, we measured the PL responses of three encapsulated alkylammonium perovskites which have excitonic absorption at ~2.5 eV. Figure 3a depicts the PL spectra of $(BA)_2PbI_4$ photoexcited by 400 nm laser pulses measured at selected temperatures. At 10 K, three resonant luminescence peaks are observed at 2.38 (P_1), 2.49 (P_2), and 2.54 (P_3) eV. As the temperature increases up to 260 K, the peak P_3 is gradually red-shifted, while the peaks P_1 and P_2 are blue-shifted. At around 280 K, a new broad peak abruptly emerges out at 2.37 eV and it remains present at higher temperatures. This abrupt shift of PL peak at near room-temperature has been observed for other layered perovskites, and it corresponds to the order-disorder structural phase transition of alkylammonium chains.[26-28] Figure 3b shows the temperature dependence of peak positions of P_1 and P_3. The red-shift of the exciton PL energy of P_3 before phase transition can be well-fitted by the Varshni equation.[29] The thermal expansion coefficient (α) obtained from fitting is $2.9\pm0.4\times10^{-4}$ eV/K. A strong excitonic emission even at room temperature indicates the stability of the exciton states in layered perovskites. In Table 1, the fitting parameters are listed with those of two other samples.

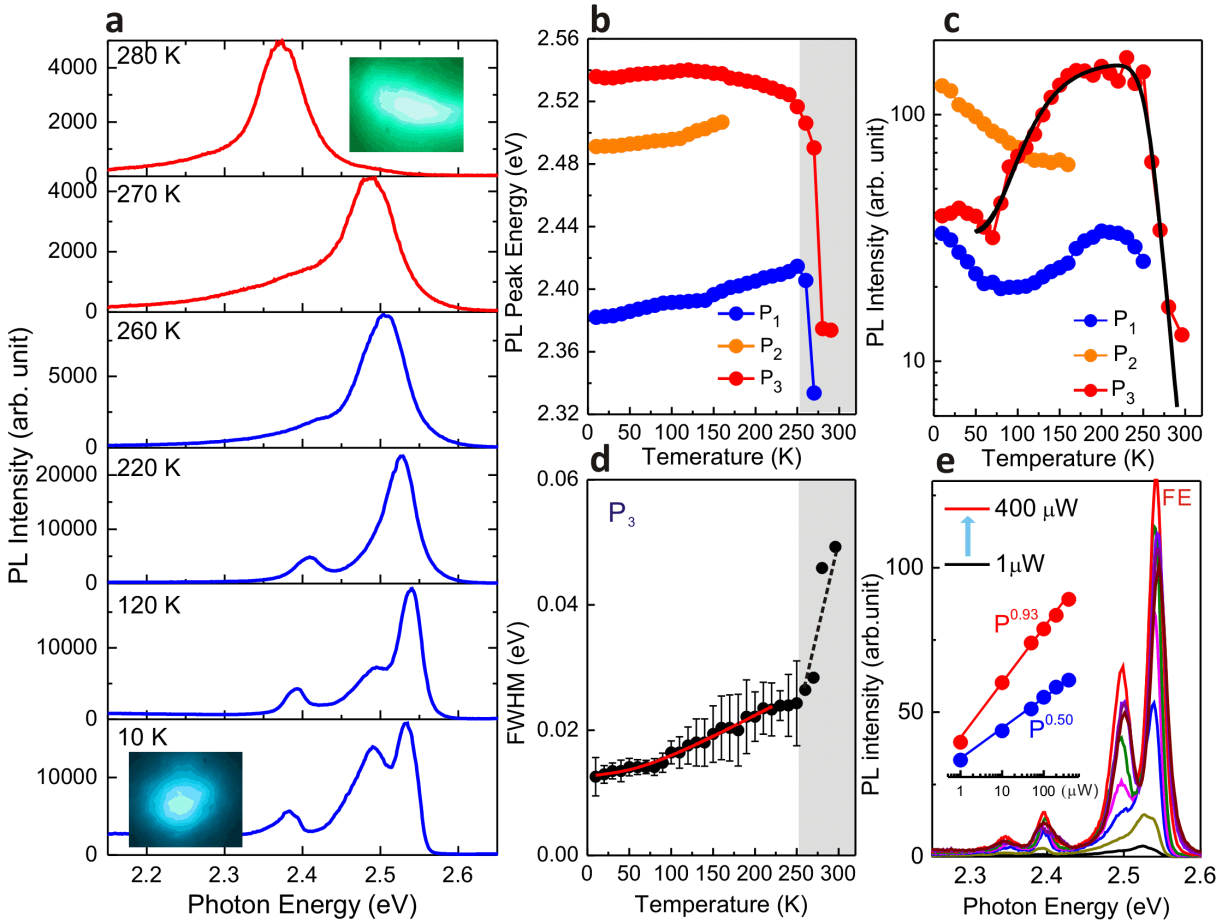

Figure 3. a. PL spectra of the encapsulated $(BA)_2PbI_4$ measured at different temperatures. Insets show the optical image of PL measured at 10 K and 280 K. **b**. and **c**. Temperature dependence of PL peak energy and intensity, respectively. **d**. Band broadening of the peak P_3 with the fitting result. **e.** Excitation power dependence of PL spectrum of $(BA)_2PbI_4$ at 120 K. Inset depicts the power-law dependence of PL intensity of P_3 (red) and P_2 (blue) on the excitation power.

Figure 3c shows the temperature dependence of integrated PL intensity of three peaks, which exhibit non-monotonic behaviors. At low temperatures (<70 K), the integrated PL intensity of P_3 is smaller than that of P_2 due to its narrow bandwidth. As the temperature increases, the PL intensity gradually increases to reach a maximum followed by the thermal quenching. At

temperatures above 200 K, the main exciton peak, P_3, quenches with an activation energy (E_a) of 658±8 meV, calculated from the best fitting with Arrhenius equation. This value is much higher than that of $MAPbI_3$ (2 – 65 meV), but agrees well with those of two-dimensional layered perovskites.[4,30] The band broadening of the peak P_3 in Figure 3d is fitted using the formula proposed by Rudin[31] and from the best fitting results, the strength of exciton phonon interaction (Γ_{op}) is estimated to be 10±6 meV and the average phonon energy ($\hbar\omega_{op}$) is ~26 meV.

The excitation power (P) dependence of PL for $(BA)_2PbI_4$ at 120 K is shown in Figure 3e. The PL spectrum under low-power excitation is similar to that in Figure 3a, but as the excitation intensity increases, the peak P_2 significantly increases compared to P_1 and P_3 and a new peak due to defects appears at 2.34 eV. In the inset, we fitted the dependence of the integrated PL intensity I on P with a power-law $I \propto P^n$, obtaining n = 0.50±0.03 for P_2 and n = 0.93±0.05 for P_3. The power index of $n \sim 1$ corresponds to the single electron-hole pair recombination process, then $n<<1$ for the peak P_2 reveals insight into another recombination process for excited carriers. Figure 3c shows that the intensity of the peak P_2 decreases rapidly as the temperature increases, implying that the peak P_2 is originated from a shallow bound exciton trapped in defects.[30,32]

Despite longer exposure to ambient conditions, the light emitting as well as optical absorption properties of the unencapsulated $(BA)_2PbI_4$ are very similar to those of the encapsulated fresh $(BA)_2PbI_4$, indicating that $(BA)_2PbI_4$ with longest alkylammonium chain among three cations is ambient stable. (see Figure S3)

Table 1. List of the best-fit parameters used in the related formulae in the text.

Sample	α [eV/K]	E_a [meV]	Γ_{op} [meV]	$\hbar\omega_{op}$ [meV]
$EAPbI_3$	5.0×10^{-4}	33	63	21

$(PA)_2PbI_4$	2.4×10^{-4}	600	13	18
$(BA)_2PbI_4$	2.9×10^{-4}	658	10	26

Figure 4 shows the temperature-dependent PL response of $EAPbI_3$. Similar to $(BA)_2PbI_4$, the low-temperature PL shows a strong narrow-band free-exciton emission at ~2.51 eV and a defect-related peak at 2.42 eV. Additionally, there is a broadband emission, which is much weaker than excitonic PL. As the temperature increases, the excitonic emission quickly quenches and only the broadband emission remains up to room temperature. Similar temperature dependence of PL has been observed for other 1D perovskites[33,34] and the enhancement of broadband emission at high temperatures is described to be due to the self-trapped excitons.[34] From the quick thermal quenching of excitonic PL intensity in Figures 4b, E_a of $EAPbI_3$ is estimated to be 33±3 meV, which is much smaller than that of $(BA)_2PbI_4$ and consistent with the presence of a small excitonic absorption peak in Figure 1b. In Figure 4c, the PL peak energy shows a monotonic dependence on temperature, different from $(BA)_2PbI_4$ with a sudden peak shift near room-temperature. Best fitting results to the peak energy and the full-width-at-half-maximum (FWHM) in Figure 4c (solid lines) are obtained with the fitting parameters of α=5.0±0.2×10^{-4} eV/K and Γ_{op} = 63±9 meV, respectively. Γ_{op} of $EAPbI_3$ is larger than that of $(BA)_2PbI_4$ (10 meV), but similar to that of $MAPbI_3$ (56 meV). This indicates that the optical properties of low-dimensional perovskites are dominated by the connectivity of octahedra and the coexistence of excitonic and broadband emission in $EAPbI_3$ is due to its 1D face-shared chain structure, in which excitons are localized in 1D chain and have stronger exciton phonon interaction as octahedra in 1D chains are more distorted.[34]

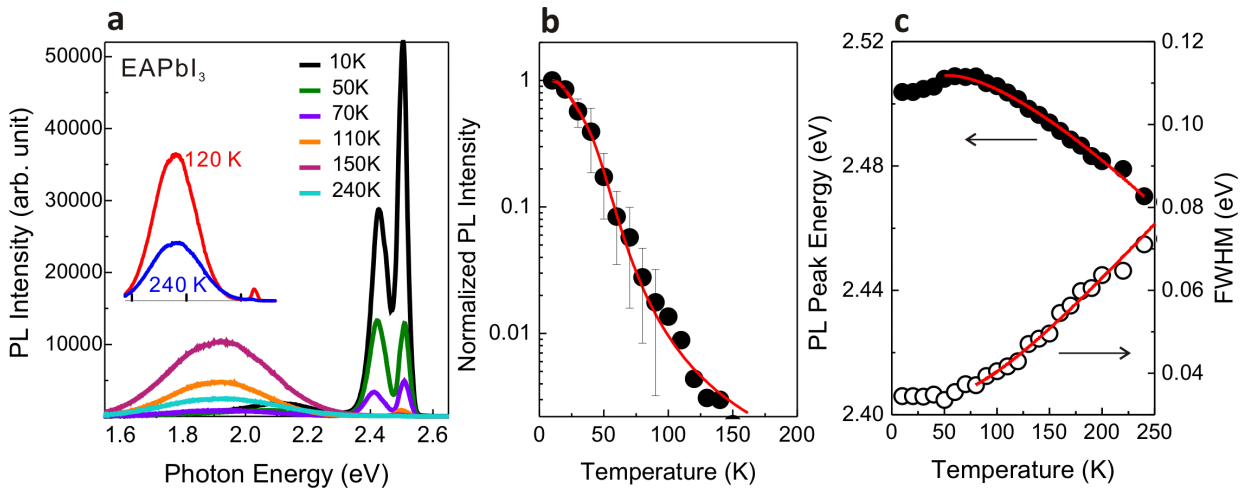

Figure 4. a. PL spectra of $EAPbI_3$ measured at different temperatures. **b.** and **c.** Temperature dependence of normalized PL intensity, PL peak energy, and FWHM of the peak at 2.51 eV. Inset shows that the free exciton emission quickly quenches as the temperature increases and only the broadband PL remains at high temperatures.

The encapsulated $(PA)_2PbI_4$ emits a strong excitonic PL at ~2.52 eV and the thermal dependence of PL is very similar to that of $(BA)_2PbI_4$, indicating that it has a similar sheet structure with tightly confined excitons (see Figure S4). At around 240 K (slightly lower temperature than $(BA)_2PbI_4$), it also undergoes the disorder-to-order phase transition and the activation energy E_a is estimated to be 600±6 meV in Figure S4c. Similar to $(BA)_2PbI_4$, there is a small peak at around 2.48 eV, due to the shallow bound exciton trapped in defects, which quickly quenches as the temperature increases. Although the PL intensity slightly decreases when measured about one month after the deposition, the intrinsic properties of the encapsulated $(PA)_2PbI_4$ samples remains the same as the fresh ones. The morphology of this sample still shows platelets similar to the one in Figure 1a.

Notably and interestingly, when $(PA)_2PbI_4$ is exposed to ambient environment, the $(PA)_2PbI_4$ without encapsulation presents significantly different emission characteristics compared to the

encapsulated $(PA)_2PbI_4$. In addition, these sample properties are dependent on the solvents (dimethyl sulfoxide (DMSO) or N-Dimethylformamide (DMF)) used, the time of ambient exposure as well as ambient humidity, as observed from Figure S5 and Figure S6. In Figure S5, it can be observed that as-prepared samples already start to exhibit some presence of deformed structure with mixed connectivity (corner- and face-sharing) as a consequence of ambient exposure. The samples prepared with higher proportion of DMSO degrade more easily, exhibiting higher and faster growing proportion of mixed connectivity phase, as observed from XRD patterns in Figure S7 and faster blue-shift of the absorption and PL spectra upon ambient exposure. All U-$(PA)_2PbI_4$ samples exhibit changes in the film morphology upon ambient exposure, crucially dependent on the time of exposure and ambient humidity levels, as observed in Figure 5 and Figure S8. After about one hour of exposure to ambient air with RH of 50%, clear transformation to nanorods can be observed for PA-based perovskite, while BA-based one remains in plate-like morphology consistent with the absence of shift in absorption or emission peaks. The transformation of perovskite platelets to wider bandgap, rod-shaped crystals was previously reported to occur in the presence of water.[7] Since the transformation of PA-based samples occurs after their exposure to ambient environment and is accelerated by increased humidity, water is most likely plays a significant role during this transformation. However, in our work water is not incorporated into the sample structure in PA-based samples, i.e. there is no evidence of hydrate formation from the XRD data in Figure 2e, and there is no significant difference in the Fourier-transformed infrared (FTIR) spectra of fresh and aged samples. (see Figure S9) In addition, partial recovery of the sample structure is possible upon annealing at temperature above 120 ºC. Figure S10 depicts the XRD data measured for as-prepared, aged, and annealed after aging samples. From the diffraction patterns of annealed samples treated at 100 °C and 120 °C, it can be noticed that

partial recovery from aged back to as-prepared structure took place upon annealing to 120 °C. This result confirms that the structural deformation is not due to the incorporation of water molecules in the crystal lattice, but instead the presence of water molecules as solvent vapor facilitates molecule mobility and structural re-arrangement. The absorption spectra, shown in Figure S11, are in good agreement with the partial recovery of the samples observed from XRD.

The structural transformation is typically accompanied by the blue-shift of the absorption edge and the PL spectra. The widening of the bandgap has been reported to occur in perovskites as a result of change in the connectivity from corner sharing via edge- to face-sharing.[7] Figure 5c exhibits that the optical absorption edge of the U-$(PA)_2PbI_4$ is shifted to higher energy (>2.8 eV) than the encapsulated $(PA)_2PbI_4$, which is then consistent with the observed change in the sample structure from 2D sheets of corner sharing lead iodide octahedral to the structure containing inorganic sheets of both corner- and face-sharing $[PbI_6]^{4-}$ octahedra.

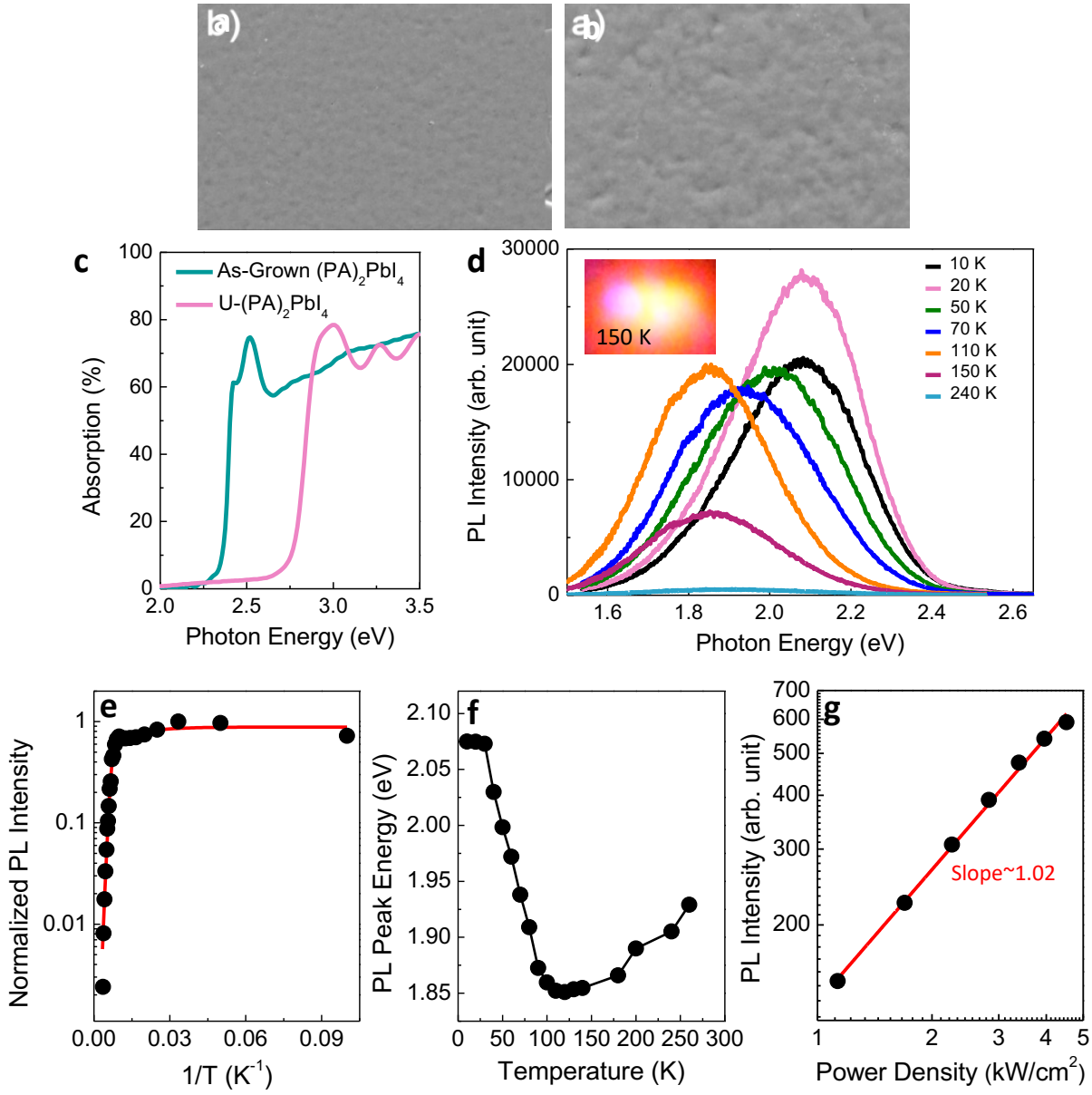

Figure 5. SEM images of the unencapsulated $(PA)_2PbI_4$ fabricated with the precursor solution of **a.** mixture of DMF:DMSO=3:1 and **b.** DMSO after one-hour exposure to ambient environment. **c.** The optical absorption spectra of the encapsulated and unencapsulated $(PA)_2PbI_4$. **d** Temperature-dependent PL spectra of the U-$(PA)_2PbI_4$. **e.** Integrated PL intensity vs. temperature. The estimated activation energy is ~120 meV. **f.** Thermal dependence of integrated PL peak energy. **g**. Integrated PL intensity vs. laser power density. The linear slope is 1.02.

More importantly, the corresponding excitonic PL is not observed at all. Instead, the PL spectra of U-$(PA)_2PbI_4$ exhibit a strong broadband emission which is largely shifted from the band edge and spans the visible spectrum from 500 nm to 800 nm. Such broadband white light emissions are occasionally observed in lead halide perovskites with lattice distortions, and can exhibit photoluminescence quantum yields (PLQYs) in the range 0.5-9%.[35,36] Our samples behave in a similar manner, with emission intensity at room temperature below the detection threshold of a PLQY setup (about 1%). As shown in Figure 5d, the broadband PL keeps its high intensity up to 120 K and gradually decreases with further increase of temperature. From the fitting to the thermal dependence of the PL intensity in Figure 5e, the activation energy E_a is estimated to be 120±10 meV, which is smaller than that of the encapsulated $(PA)_2PbI_4$, but is still much higher than those of $MAPbI_3$ and $EAPbI_3$. This result indicates that excitons in the aged $(PA)_2PbI_4$ are still localized. Furthermore, Figure S12 shows that broadband PL is even enhanced and stable as the ambient exposure increases.

In Figure 5f, the thermal evolution of PL peak energy of U-$(PA)_2PbI_4$ is also significantly different from that of the encapsulated $(PA)_2PbI_4$ in such a way that it first red-shifts at low temperatures and gradually blue-shifts as the temperature increases above ~100 K. Similar blue-shift of PL peak energy with the increase of temperature is observed for $MAPbI_3$ in the tetragonal phase above 160 K, corresponding to the distortion of octahedra due to the enhanced electron-phonon interaction at high temperatures.[37] (see Figure S13) Therefore, the observed anomalous blue-shift of emission peak as well as the broadband emission in $(PA)_2PbI_4$ can be postulated to be related to the enhanced lattice distortion.

Furthermore, the PL intensity shows a linear dependence (n=1.02) on the excitation power in Figure 5g, confirming that the broadband PL from $(PA)_2PbI_4$ is not attributed to intrinsic defects

in the crystal.[14] While the broadband emission at low temperatures in $MAPbI_3$ with similar power dependence has been previously assigned to be due to bound excitons,[38] this emission lacks the complex peak energy dependence on the temperature observed in $(PA)_2PbI_4$ samples. Recently, the structural distortion as well as the similar broadband emission has been reported for various 2D lead-halide perovskites. And a series of extensive research revealed that the exciton self-trapping due to structural distortion of octahedra PbI_6 is responsible for the broadband emission from those layered perovskites, and the broadband emission is critically dependent on the choice of organic cations.[10-15] We note that no broadband emission as well as the ambient stability was previously reported for a perovskite with simple alkyl ammonium spacer cation, such as PA. Since the broadband emission from U-$(PA)_2PbI_4$ is still excitonic and it is enhanced with increased ambient exposure, it can be attributed to self-trapped excitons at structural deformations induced by transformation from layers of corner-sharing octahedra to mixed connectivity containing both corner-sharing and face-sharing octahedra.

CONCLUSIONS

In order to address the optical properties for alkylammonium lead iodides, three shortest alkylammonium cations were introduced to synthesize low-dimensional perovskites. The fabricated $EAPbI_3$ is crystalized to a long chain-like 1D structure which consists of only face-sharing PbI_6 octahedra. Despite strong excitonic emission at ~2.5 eV, its thermal properties are found to be closer to those of a 3D perovskite, $MAPbI_3$, rather than 2D counterparts. Crystallographic analysis shows that as-prepared fresh $(PA)_2PbI_4$ and $(BA)_2PbI_4$ have the Ruddlesden–Popper structures with uniformly flat corner-sharing octahedral layers. Due to the well-separated organic barriers, both 2D perovskites have very high exciton binding energies (>600 meV) and emit strong and narrow free-exciton emission. While $(BA)_2PbI_4$ with the longest

alkylammonium cations has high ambient stability, $(PA)_2PbI_4$ exposed to air without encapsulation undergoes notable changes in structural and optical properties. XRD analysis clearly shows that two-dimensional layer structure with corner-sharing octahedra evolves to a deformed structure of mixed connectivity containing both corner-sharing and face-sharing octahedra and the aged $(PA)_2PbI_4$ emits broadband PL covering the visible spectrum from 500 nm to 800 nm. High exciton binding energy and the linear power dependence of PL indicate that this broadband emission is attributed to the formation of self-trapped excitons due to the structural deformation. Our results show how ambient aging causes the structural deformation which affects the direct tuning of optical properties in 2D organic/inorganic hybrid perovskites.

EXPERIMENTAL SECTION

Fabrication procedures for 2D & 3D perovskite films. N, N-Dimethylformamide (DMF, anhydrous, 99.9+%), dimethyl sulfoxide (DMSO, anhydrous, 99.8+%), and lead iodide (PbI_2, 99.9985%) are purchased from Alfa Aesar. Methylammonium iodide, ethylammonium iodide, n-propylammonium iodide, and n-butylammonium iodide are purchased from Great cell Solar Ltd. Quartz encapsulating cover and ITO/glass substrates are cleaned by sonication for 10 min. in acetone, toluene, acetone, ethanol, and deionized water respectively, and followed by oxygen plasma treatment immediately before use. Precursor solutions for different perovskites are prepared by dissolving the precursor materials in a mixture of DMF and DMSO at a concentration of 0.5 M. For $MAPbI_3$, PbI_2 and MAI are dissolved in molar ratio of 1:1 in the mixture of DMF and DMSO (7:3 volume ratio). For $EAPbI_3$, PbI_2 and EAI are dissolved in molar ratio of 1:1 in the mixture of DMF and DMSO (5:1 volume ratio). For $(PA)_2PbI_4$ and $(BA)_2PbI_4$, PbI_2 and the corresponding ammonium iodide salt are dissolved in molar ratio of 2:1 in the mixture of DMF and DMSO (3:1 volume ratio). The perovskite films are prepared by spin-coating the precursor

solutions inside an argon-filled glovebox. For $MAPbI_3$, the precursor solution is spin-coated at 5000 rpm for 30 s, with chlorobenzene dripped on the substrate by the last 10 s of the spinning process. For $EAPbI_3$, PA_2PbI_4, and BA_2PbI_4, the precursor solution is spin-coated at 5000 rpm for 30 s. The sample was transferred to a vacuum chamber immediately after spin-coating and kept in vacuum for 1 minute. All the perovskite films were annealed at 120 °C for 10 min to remove the solvent thoroughly. Sample aging was performed in ambient for a specified time and ambient humidity. To test the structural recovery upon annealing, aged samples were further annealed at 100 ºC or 120 ºC in ambient for 5 mins.

Optical Measurement. Low-temperature PL measurements were performed by using a low-vibration, closed-cycle cryostats system (attocube, AttoDRY800) with a 100× objective lens (attocube, LT-APO/VIS, N.A.=0.82) inside the vacuum chamber. We used a pulsed semiconductor diode laser at 405 nm (PicoQuant LDH P-C-405B; 40 MHz, 40 ps) as the optical excitation source with a spot size about 3 μm. The laser power used for the power dependence of PL measurement is 1 – 400 μW. The optical excitation and collection of emission from the samples were carried out using the same objective lens at normal incidence, and the emission signal was dispersed by a homebuilt spectrometer equipped with a TE-cooled CCD (Andor, iDus 420). The Raman spectra were measured by excitation of the samples with a CW 532 nm laser (Cobolt Samba, 05-01). A Bragg filter was used to block the excitation laser line, enabling the measurement from ~50 cm^{-1}. The morphologies of perovskites were analyzed by SEM (JEOL, JSM-7000F). XRD θ-2θ scans (Bede D1 HR-XRD) of perovskite films deposited on ITO substrates were performed using an XRD diffractometer with monochromatic Cu-Kα radiation (λ = 1.5406 Å) to characterize the reflections along the surface normal. Attenuated total reflection Fourier transform infrared

spectroscopy (ATR-FTIR) measurements were performed using a PerkinElmer Spectrum Two UATR Two Spectrometer.

ASSOCIATED CONTENT

Supporting Information. Additional PL, XRD, and optical absorption spectra, SEM images, crystal structure schematic diagram and FTIR spectra of aged $(PA)_2PbI_4$. The Supporting Information is available free of charge.

AUTHOR INFORMATION

Corresponding Author

* Tel) +886 3571 2121, Fax) +886 3571 6631, E-mail) hyahn@mail.nctu.edu.tw

* Tel) +852 2859 7946, Fax) +852 2559 9152, E-mail) dalek@hku.hk

ACKNOWLEDGMENT

H.A. acknowledges financial support from the Ministry of Science and Technology (MOST 107-2112-M-009-015-MY3 and MOST 107-2923-M-009-003-MY3) of Taiwan. A.D. thanks the financial support from the Natural Science Foundation of Shenzhen Innovation Committee (JCYJ20170818141216288), RGC CRF grant 5037/18G and Seed Funding for basic research of the University of Hong Kong.

ABBREVIATIONS

2D, two-dimensional; PCE, power conversion efficiency; MA, methylammonium; EA, mono-ethylammonium; PA, n-propylammonium; BA, n-butylammonium; PL, photoluminescence; XRD, X-ray diffraction; FWHM, full-width-at-half-maximum; DMF, N-Dimethylformamide;

DMSO, dimethyl sulfoxide; R-P, Ruddlesden–Popper; FTIR, Fourier-transformed infrared spectroscopy.

REFERENCES

1. https://www.nrel.gov/pv/assets/pdfs/best-research-cell-efficiencies-190416.pdf.
2. Peterson E. R.; Willett R. D. Crystal Structure of $(CH_3CH_2CH_2NH_3)_2MnCl_4$, *J. Chem. Phys.* **1972**, *56*, 1879−1882.
3. Safdari, M.; Fischer, A.; Xu, B.; Kloo, L.; Gardner, J. M. Structure and Function Relationships in Alkylammonium Lead(II) Iodide Solar Cells, *J. Mater. Chem. A*, **2015**, *3*, 9201−9207.
4. Li, B.; Fei, C.; Zheng, K.; Qu, X.; Pullerits, T.; Cao, G.; Tian J. Constructing Water-Resistant $CH_3NH_3PbI_3$ Perovskite Films *via* Coordination Interaction, *J. Mater. Chem. A*, **2016**, *4*, 17018–17024.
5. Lode, C.; Krautscheid, H. Iodostannates with Polymeric Anions: $(Me_3PhN)_2^{1\infty}[Sn_3I_{10}]$, $[Me_2HN\text{-}(CH_2)_2\text{-}NMe_2H]_2^{1\infty}[Sn_3I_{10}]$, $[Me_2HN\text{-}(CH_2)_2\text{-}NMe_2H]_2^{1\infty}[Sn_3I_8]$, *Z. Anorg. Allg. Chem.* **2001**, *627*, 1454−1458.
6. Im, H.; Chung, J.; Kim, S.-J.; Park, N.-G. Synthesis, Structure, and Photovoltaic Property of a Nanocrystalline 2H Perovskite-Type Novel Sensitizer $(CH_3CH_2NH_3)PbI_3$, *Nanoscale Res. Lett.*, **2012**, *7*, 353.
7. Kamminga, M. E.; Fang, H.-H.; Filip, M. R.; Giustino, F.; Baas, J.; Blake, G. R.; Loi, M. A.; Palstra, T. T. M. Confinement Effects in Low-Dimensional Lead Iodide Perovskite Hybrids. *Chem. Mater.* **2016**, *28*, 4554−4562.
8. Hoffman, J. M.; Che, X.; Sidhik, S.; Li, X.; Hadar, I.; Blancon, J.-C.; Yamaguchi, H.; Kepenekian, M.; Katan, C.; Even, J.; Stoumpos, C. C.; Mohite, A. D.; Kanatzidis, M. G.

From 2D to 1D Electronic Dimensionality in Halide Perovskites with Stepped and Flat Layers using Propylammonium as a Spacer, *J. Am. Chem. Soc.* **2019**, *141*, 10661–10676.

9. Yao, D.; Zhang, C.; Zhang, S.; Yang, Y.; Du, A.; Waclawik, E.; Yu, X.; Wilson, G. J.; Wang H. 2D−3D Mixed Organic−Inorganic Perovskite Layers for Solar Cells with Enhanced Efficiency and Stability Induced by n-Propylammonium Iodide Additives, *ACS Appl. Mater. Interfaces* **2019**, *11*, 29753−29764.
10. Cortecchia, D.; Neutzner, S.; Kandada, A. R. S.; Mosconi, E.; Meggiolaro, D.; Angelis, R. D.; Soci, C.; Petrozza, A. Broadband Emission in Two-Dimensional Hybrid Perovskites: The Role of Structural Deformation, *J. Am. Chem. Soc.* **2017**, *139*, 39−42.
11. Yangui, A.; Garrot, D.; Lauret, J. S.; Lusson, A.; Bouchez, G.; Deleporte, E.; Pillet, S.; Bendeif, E. E.; Castro, M.; Triki, S.; Abid, Y.; Boukheddaden, K. Optical Investigation of Broadband White-Light Emission in Self-Assembled Organic−Inorganic Perovskite $(C_6H_{11}NH_3)_2PbBr_4$, *J. Phys. Chem. C* **2015**, *119*, 23638–23647.
12. Hu, T.; Smith, M. D.; Dohner, E. R.; Sher, M.-J.; Wu, X.; Trinh, M. T.; Fisher, A.; Corbett, J.; Zhu, X. Y.; Karunadasa, H. I.; Lindenberg, A. M. Mechanism for Broadband White-Light Emission from Two-Dimensional (110) Hybrid Perovskites, *J. Phys. Chem. Lett.,* **2016**, *7*, 2258–2263.
13. Cortecchia, D.; Yin, J.; Bruno, A.; Lo, S.-Z. A.; Gurzadyan, G. G.; Mhaisalkar, S.; Bre'das, J. L. Soci, C. Polaron Self-Localization in White-Light Emitting Hybrid Perovskites, *J. Mater. Chem. C,* **2017**, *5*, 2771−2780.
14. Smith, M. D.; Jaffe, A.; Dohner, E. R.; Lindenberg, A. M.; Karunadasa, H. I. Structural Origins of Broadband Emission from Layered Pb−Br Hybrid Perovskites, *Chem. Sci.* **2017**, *8*, 4497−4504.

15. Smith, M. D.; Karunadasa, H. I. White-Light Emission from Layered Halide Perovskites, *Acc. Chem. Res*. **2018**, *51*, 619−627.

16. Mitzi, D. B. Templating and Structural Engineering in Organic−Inorganic Perovskites. *J. Chem. Soc., Dalton Trans.* **2001**, 1−12.

17. Cho, J.; Choi, Y. H.; O'Loughlin, T. E.; De Jesus, L.; Banerjee, S. Ligand-Mediated Modulation of Layer Thicknesses of Perovskite Methylammonium Lead Bromide Nanoplatelets, *Chem. Mater.* **2016,** *28*, 6909–6916.

18. Gao, P.; Yusoff, A. R. B. M.; Nazeeruddin, M. K. Dimensionality Engineering of Hybrid Halide Perovskite Light Absorbers, *Nat. Commun*. **2018**, *9*, 5028.

19. Aharon, S.; Wierzbowska, M.; Etgar, L. The Effect of the Alkylammonium Ligand's Length on Organic-Inorganic Perovskite Nanoparticles, *ACS Energy Lett*. **2018**, *3*, 1387−1393.

20. Quarti, C.; Grancini, G.; Mosconi, E.; Bruno, P.; Ball, J. M.; Lee, M. M.; Snaith, H. J.; Petrozza, A.; Angelis, F. D. The Raman Spectrum of the $CH_3NH_3PbI_3$ Hybrid Perovskite: Interplay of Theory and Experiment, *J. Phys. Chem. Lett*. **2014**, *5*, 279−284.

21. Brivio, F.; Frost, J. M.; Skelton, J. M.; Jackson, A. J.; Weber, O. J.; Weller, M. T.; Goni, A. R.; Leguy, A. M. A.; Barnes, P. R. F.; Walsh, A. Lattice Dynamics and Vibrational Spectra of the Orthorhombic, Tetragonal, and Cubic Phases of Methylammonium Lead Iodide, *Phys. Rev. B: Condens. Matter Mater. Phys.* **2015**, *92*, 144308.

22. Yamada, Y.; Yamada, T.; Phuong, L. Q.; Maruyama, N.; Nishimura, H.; Wakamiya, A.; Murata Y.; Kanemitsu, Y. Dynamic Optical Properties of $CH_3NH_3PbI_3$ Single Crystals as Revealed by One- and Two-Photon Excited Photoluminescence Measurements, *J. Am. Chem. Soc.* **2015**, *137*, 10456−10459.

23. Dou L.; Wong A. B.; Yu Y.; Lai M.; Kornienko N.; Eaton S. W.; Fu A.; Bischak C. G.; Ma J.; Ding T.; Ginsberg N. S.; Wang L. W.; Alivisatos A. P.; Yang P. Atomically Thin Two-Dimensional Organic-Inorganic Hybrid Perovskites, *Science* **2015**, *349*, 1518−1521.

24. Meresse, A.; Doud, A. Bis(n-propylammonium) Tetrachloroplumbate, *Acta Cryst*. **1989**, *C45*, 194−196.

25. Billing, D. G.; Lemmerer, A. Octakis(3-propyl-ammonium) Octadecaiodopentaplumbate(II): a New Layered Stucture based on Layered Perovskites, *Acta Cryst.* **2006**, *C62*, m238–m240.

26. Mokhlisse, R.; Couzi, M.; Chanh, N. B.; Haget, Y.; Hauw C.; Meresse, A. Raman Scattering and X-ray Diffraction Study of Structural Phase Transitions in the Perovskite-Type Layer Compound $(C_3H_7NH_3)_2CdCl_4$, *J. Phys. Chem. Solids*, **1985**, *46*, 187–195.

27. Billing, D. G.; Lemmerer, A. Synthesis, Characterization and Phase Transitions in the Inorganic–Organic Layered Perovskite-Type Hybrids $[(C_nH_{2n+1}NH_3)_2PbI_4]$, n = 4, 5 and 6, *Acta Cryst*. **2007,** *B63,* 735–747.

28. Ni, L.; Huynh,U.; Cheminal, A.; Thomas, T. H.; Shivanna, R.; Hinrichsen, T. F.; Ahmad, S.; Sadhanala, A.; Rao, A. Real-Time Observation of Exciton−Phonon Coupling Dynamics in Self-Assembled Hybrid Perovskite Quantum Wells, *ACS Nano* **2017**, *11*, 10834−10843.

29. Varshni, Y. P. Temperature Dependence of the Energy Gap in Semiconductors, *Physica*, **1967**, *34*, 149−154.

30. Ishihara, T.; Takahashi, J.; Goto, T. Optical Properties due to Electronic Transitions in Two-Dimensional Semiconductors $(C_nH_{2n+1}NH_3)_2PbI_4$, *Phys. Rev. B*, **1990**, *42*, 11099–11107.

31. Rudin, S.; Reinecke, T. L.; Segall, B. Temperature-Dependent Exciton Linewidths in Semiconductors, *Phys. Rev. B: Condens. Matter* **1990**, *42*, 11218−11231.

32. Wu, X.; Trinh, M. T.; Niesner, D.; Zhu, H.; Norman, Z.; Owen, J. S.; Yaffe, O.; Kudisch, B. J.; Zhu X.-Y. Trap States in Lead Iodide Perovskites, *J. Am. Chem. Soc.* **2015**, *137*, 2089−2096.

33. Tong, Y.-B.; Ren, L.-T.; Duan, H.-B.; Liu, J.-L.; Ren, X.-M. An Amphidynamic Inorganic–Organic Hybrid Crystal of Bromoplumbate with 1,5-Bis(1-methylimidazolium)pentane Exhibiting Multi-Functionality of a Dielectric Anomaly and Temperature-Dependent Dual Band Emissions, *Dalton Trans.* **2015**, *44*, 17850−17858.

34. Mao, L.; Guo, P.; Kepenekian, M.; Hadar, I.; Katan, C.; Even, J.; Schaller, R. D.; Stoumpos, C. C.; Kanatzidis, M. G. Structural Diversity in White-Light-Emitting Hybrid Lead Bromide, *J. Am. Chem. Soc.* **2018**, *140*, 13078−13088.

35. Brochard-Garnier, S.; Paris, M.; Génois, R.; Han, Q. X.; Liu, Y.; Massuyeau, F.; Gautier, R. Screening Approach for the Discovery of New Hybrid Perovskites with Efficient Photoemission. *Adv. Funct. Mater.* **2019**, *29*, 1806728.

36. Gautier, R.; Massuyeau, F.; Galnon, G.; Paris, M. Lead Halide Post-Perovskite-Type Chains for High-Efficiency White-Light Emission. *Adv. Mater.* **2019**, *31*, 1807383.

37. Singh, S.; Li, C.; Panzer, F.; Narasimhan, K. L.; Graeser, A.; Gujar, T. P.; Köhler, A.; Thelakkat, M.; Huettner, S.; Kabra, D. Effect of Thermal and Structural Disorder on the Electronic Structure of Hybrid Perovskite Semiconductor $CH_3NH_3PbI_3$, *J. Phys. Chem. Lett.* **2016**, *7*, 3014−3021.

38. Fang, H.-H.; Raissa, R.; Abdu-Aguye, M.; Adjokatse, S.; Blake, G. R.; Jacky Even, J.; Loi, M. A. Photophysics of Organic–Inorganic Hybrid Lead Iodide Perovskite Single Crystals, *Adv. Funct. Mater.* **2015**, *25*, 2378–2385.

Table of Contents graphic